J|A|C|S
A R T I C L E S

Microporous Metal−Organic Frameworks Incorporating 1,4-Benzeneditetrazolate: Syntheses, Structures, and Hydrogen Storage Properties

Mircea Dincă, Anta F. Yu, and Jeffrey R. Long*

Contribution from the Department of Chemistry, University of California, Berkeley, California 94720

Received March 12, 2006; E-mail: jrlong@berkeley.edu

Abstract: The potential of tetrazolate-based ligands for forming metal−organic frameworks of utility in hydrogen storage is demonstrated with the use of 1,4-benzeneditetrazolate (BDT^{2-}) to generate a series of robust, microporous materials. Reaction of H_2BDT with $MnCl_2 \cdot 4H_2O$ and $Mn(NO_3)_2 \cdot 4H_2O$ in *N,N*-diethylformamide (DEF) produces the two-dimensional framework solids $Mn_3(BDT)_2Cl_2(DEF)_6$ (**1**) and Mn_4-$(BDT)_3(NO_3)_2(DEF)_6$ (**2**), whereas reactions with hydrated salts of Mn^{2+}, Cu^{2+}, and Zn^{2+} in a mixture of methanol and DMF afford the porous, three-dimensional framework solids $Zn_3(BDT)_3(DMF)_4(H_2O)_2 \cdot 3.5CH_3$-$OH$ (**3**), $Mn_3(BDT)_3(DMF)_4(H_2O)_2 \cdot 3CH_3OH \cdot 2H_2O \cdot DMF$ (**4**), $Mn_2(BDT)Cl_2(DMF)_2 \cdot 1.5CH_3OH \cdot H_2O$ (**5**), and Cu-$(BDT)(DMF) \cdot CH_3OH \cdot 0.25DMF$ (**6**). It is shown that the method for desolvating such compounds can dramatically influence the ensuing gas sorption properties. When subjected to a mild evacuation procedure, compounds **3**−**6** exhibit permanent porosity, with BET surface areas in the range 200−640 m^2/g. The desolvated forms of **3**−**5** store between 0.82 and 1.46 wt % H_2 at 77 K and 1 atm, with enthalpies of adsorption in the range 6.0−8.8 kJ/mol, among the highest so far reported for metal−organic frameworks. In addition, the desolvated form of **6** exhibits preferential adsorption of O_2 over H_2 and N_2, showing promise for gas separation and purification applications.

Introduction

Situated at the confluence of materials science, solid-state chemistry, and coordination chemistry, the study of microporous metal−organic frameworks has developed into an intense field of chemical research. The first metal−organic frameworks, reported by Robson and others in the early 1990s, typically consisted of single metal ions connected by simple tetrahedral or rod-shaped ligands, such as tetracyanophenylmethane or 4,4'-bipyridine,[1] and had little or no practical applicability. The use of more varied organic linkers and the replacement of single metal ions with metal clusters, however, has since led to the synthesis of increasingly complex frameworks with a variety of proposed applications.[2] Recently, structure predictability, an important requirement for the synthesis of functional materials with tailored properties, has even become possible, in many cases by combining topological principles laid out by Wells[3]

with new computational models.[4] In all, the combined knowledge accumulated in the field over the last fifteen years has enabled the synthesis of a new generation of microporous materials with potential applications in magnetism,[5] catalysis,[6] luminescence and chemical sensing,[7] and gas adsorption and/or separation.[8]

Microporous metal−organic frameworks exhibiting large surface areas and permanent porosity have also achieved recent prominence due to their potential as hydrogen storage materials for mobile applications. The initial finding of reversible hydrogen adsorption in $Zn_4O(BDC)_3$ (BDC = 1,4-benzenedicarboxylate)[9] was followed by numerous reports of other

(1) (a) Hoskins, B. F.; Robson, R. *J. Am. Chem. Soc.* **1989**, *111*, 5962−5964. (b) Hoskins, B. F.; Robson, R. *J. Am. Chem. Soc.* **1990**, *112*, 1546−1554. (c) Abrahams, B. F.; Hoskins, B. F.; Liu, J. L.; Robson, R. *J. Am. Chem. Soc.* **1991**, *113*, 3045−3051. (d) Abrahams, B. F.; Hoskins, B. F.; Robson, R. *J. Am. Chem. Soc.* **1991**, *113*, 3606−3607. (e) Fujita, M.; Kwon, Y. J.; Washizu, S.; Ogura, K. *J. Am. Chem. Soc.* **1994**, *116*, 1151−1152.

(2) Relevant reviews: (a) Moulton, B.; Zaworotko, M. J. *Chem. Rev.* **2001**, *101*, 1629−1658. (b) Eddaoudi, M.; Moler, D. B.; Li, H.; Chen, B.; Reineke, T. M.; O'Keeffe, M.; Yaghi, O. M. *Acc. Chem. Res.* **2001**, *34*, 319−330. (c) Janiak, C. *Dalton Trans.* **2003**, 2781−2804. (d) Kitagawa, S.; Kitaura, R.; Noro, S.-I. *Angew. Chem., Int. Ed.* **2004**, *43*, 2334−2375. (e) Ockwig, N. W.; Delgado-Friedrichs, O.; O'Keeffe, M.; Yaghi, O. M. *Acc. Chem. Res.* **2005**, *38*, 176−182.

(3) Wells, A. F. *Structural Inorganic Chemistry,* 5th ed.; Oxford University Press: Oxford, 1984.

(4) (a) Mellot-Draznieks, C.; Newsam, J. M.; Gorman, A. M.; Freeman, C. M.; Férey, G. *Angew. Chem., Int. Ed.* **2000**, *39*, 2270−2275. (b) Mellot-Draznieks, C.; Girard, S.; Férey, G.; Schön, J. C.; Cancarevic, Z.; Jansen, M. *Chem.−Eur. J.* **2002**, *8*, 4103−4113. (c) Férey, G.; Serre, C.; Mellot-Draznieks, C.; Millange, F.; Surblé, S.; Dutour, J.; Margiolaki, I. *Angew. Chem., Int. Ed.* **2004**, *43*, 6296−6301.

(5) (a) Rujiwatra, A.; Kepert, C. J.; Claridge, J. B.; Rosseinsky, M. J.; Kumagai, H.; Kurmoo, M. *J. Am. Chem. Soc.* **2001**, *123*, 10584−10594. (b) Beauvais, L. G.; Long, J. R. *J. Am. Chem. Soc.* **2002**, *124*, 12096−12097. (c) Maspoch, D.; Ruiz-Molina, D.; Wurst, K.; Domingo, N.; Cavallini, M.; Biscarini, F.; Tejada, J.; Rovira, C.; Veciana, J. *Nature Mater.* **2003**, *2*, 190−195. (d) Xiang, S.; Wu, X.; Zhang, J.; Fu, R.; Hu, S.; Zhang, X. *J. Am. Chem. Soc.* **2005**, *127*, 16352−16353. (e) Beauvais, L. G.; Long, J. R. *Inorg. Chem.* **2006**, *45*, 236−243.

(6) (a) Seo, J. S.; Whang, D.; Lee, H.; Jun, S. I.; Oh, J.; Jeon, Y. J.; Kim, K. *Nature* **2000**, *404*, 982. (b) Guillou, N.; Forster, P. M.; Gao, Q.; Chang, J. S.; Nogues, M.; Park, S.-E.; Cheetham, A. K.; Férey, G. *Angew. Chem., Int. Ed.* **2001**, *40*, 2831−2834. (c) Wu, C.-D.; Hu, A.; Zhang, L.; Lin, W. *J. Am. Chem. Soc.* **2005**, *127*, 8940−8941.

(7) (a) Beauvais, L. G.; Shores, M. P.; Long, J. R. *J. Am. Chem. Soc.* **2000**, *122*, 2763−2772. (b) Jianghua, H.; Jihong, Y.; Yuetao, Z.; Qinhe, P.; Ruren, X. *Inorg. Chem.* **2005**, *44*, 9279−9282.

carboxylate-based frameworks displaying significant storage capacities.[10] However, with the exceptions of the recently reported compounds [Ni₂(4,4′-bipy)₃](NO₃)₄[10c] and M(2-pymo)₂ (M = Cu, Pd; 2-pymo = 2-pyrimidinolate),[11] there are no examples of carboxylate-free metal–organic frameworks exhibiting H₂ adsorption, suggesting that the synthesis of materials based on new types of bridging ligands may yield quite different storage capabilities. The highest reported H₂ uptake for a metal–organic framework at 77 K and 1 atm is 2.47 wt %, as observed in Cu₂(BPTC) (BPTC = 3,3′,5,5′-biphenyltetracarboxylate).[10i] In contrast, Zn₄O(BDC)₃ has an adsorption capacity of 1.3 wt % at 77 K and 1 atm. One key feature that characterizes most metal–organic framework materials is the relatively low enthalpy of adsorption change associated with the H₂ uptake. This energy usually lies in the range 4.7–7.5 kJ/mol, significantly lower than the estimated 15 kJ/mol required for reversible H₂ uptake at 298 K and fuel-cell operating pressures between 1.5 and 30 atm.[12] Consequently, we are focusing on the use of alternative bridging ligands in synthesizing microporous frameworks that may exhibit higher enthalpies of adsorption, without sacrificing important features such as thermal and mechanical stability.

As a result of its simplicity and thermal robustness, Zn₄O-(BDC)₃ remains one of the most studied microporous metal–organic frameworks. This compound likely owes its unusual thermal stability to the tetrahedral Zn₄O(O₂C-)₆ units that form connecting nodes within its three-dimensional cubic framework. Notably, zinc and beryllium have long been known to form molecular analogues of the type M₄O(O₂C–R)₆ with a variety of carboxylates,[13] whereas analogous μ_4-oxo hexacarboxylate clusters of other metals are not known.[14] Attempts to design new microporous materials with properties resembling those of Zn₄O(BDC)₃ prompted us to look for other ligands that might stabilize tetrahedral [M₄O]⁶⁺ cores. A survey of the literature revealed that other metals can indeed form such species when
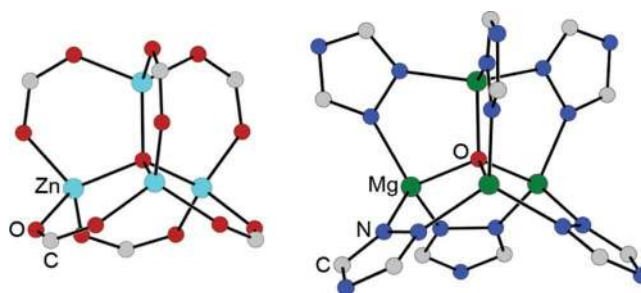

Figure 1. Structures of a Zn₄O(O₂C-)₆ unit from Zn₄O(BDC)₃ and Mg₄O(ⁱ-ptrz)₆ (ⁱptrz = 3,5-diisopropyl-1,2,4-triazole);[8a,15b] for clarity, isopropyl groups are omitted from the depiction of the latter. Selected mean interatomic distances (Å) and angles (deg): Zn–O, 1.941; Mg–O, 1.941; O···O, 2.330; N–N, 1.401; Zn–O(μ_4)-Zn, 109.47; Mg–O(μ_4)-Mg, 109.47; O(μ_4)-Zn–O, 112.65; O(μ_4)-Mg–N, 99.89; O–Zn–O, 106.12; N–Mg–N, 117.12.

the bridging carboxylate ligands are replaced by N-bound heterocyclic ligands. Specifically, molecules of the type M₄O-(az)₆ (M = Mg, Co; az = 3,5-diisopropyl-1,2,4-triazolate or 3,5-dimethylpyrazolate)[15] possess tetrahedral core geometries closely mimicking that of the [Zn₄O]⁶⁺ cluster (see Figure 1). Analogous to the carboxylate example, it is conceivable that replacing monoazolates with bridging diazolate ligands might connect [Mg₄O]⁶⁺ clusters to form lighter-weight cubic frameworks that otherwise could have similar properties to Zn₄O-(BDC)₃. Moreover, due to a shorter N–N distance in triazole compared to the O···O separation in a carboxylate, the metal centers in a tetrahedral M₄O(az)₆ unit would be much more exposed to an H₂ molecule that approaches the cluster from a direction perpendicular to the plane formed by three N atoms on adjacent triazole rings. These exposed metal centers might therefore provide stronger binding sites for adsorbed H₂ molecules.

To find a suitable substitute for linear dicarboxylates, we considered a series of diazolate ligands. Tetrazoles have long been used as carboxylic acid analogues in biological chemistry because their pK_a values are close to those of carboxylic acids ($pK_a \approx 4$).[16] Although a few tetrazolate-based coordination solids have been reported,[17] the coordination chemistry of polytopic tetrazolate ligands remains largely unexplored. The linear ditetrazole 1,4-benzeneditetrazol-5-yl (H₂BDT) was therefore investigated to determine the extent to which it might mimic H₂BDC. Herein, we report the successful incorporation of BDT²⁻ into porous, three-dimensional framework solids exhibiting reversible H₂ uptake with enhanced binding enthalpies.

Experimental Section

The compound 1,4-benzeneditetrazol-5-yl (H₂BDT) was prepared as described previously.[17d] For the synthesis of **1** and **2**, *N,N*-diethylformamide (DEF) was dried over 3 Å molecular sieves for 3 days prior to use and deoxygenated via three cycles of freezing and thawing under dynamic vacuum. All other reagents were obtained from commercial vendors and, unless otherwise noted, were used without further purification.

Mn₃(BDT)₂Cl₂(DEF)₆ (1). Solid MnCl₂·4H₂O (20 mg, 0.10 mmol) was added to a solution of H₂BDT (21 mg, 0.10 mmol) in 4 mL of DEF in a Pyrex tube (1.0 × 1.2 × 16 cm, i.d. × o.d. × length), and the mixture was degassed by four freeze–pump–thaw cycles. The tube

(8) (a) Li, H.; Eddaoudi, M.; O'Keeffe, M.; Yaghi, O. M. *Nature* **1999**, *402*, 276–279. (b) Mori, W.; Sato, T.; Ohmura, T.; Nozaki Kato, C.; Takei, T. *J. Solid State Chem.* **2005**, *178*, 2555–2573. (c) Matsuda, R.; Kitaura, R.; Kitagawa, S.; Kubota, Y.; Belosludov, R. V.; Kobayashi, T. C.; Sakamoto, H.; Chiba, T.; Takata, M.; Kawazoe, Y.; Mita, Y. *Nature* **2005**, *436*, 238–241. (d) Pan, L.; Olson, D. H.; Ciemnolonski, L. R.; Heddy, R.; Li, J. *Angew. Chem., Int. Ed.* **2006**, *46*, 616–619. (e) Mueller, U.; Schubert, M.; Teich, F.; Puetter, H.; Schierle-Arndt, K.; Pastré, J. *J. Mater. Chem.* **2006**, *16*, 626–636.
(9) (a) Rosi, N. L.; Eckert, J.; Eddaoudi, M.; Vodak, D. T.; Kim, J.; O'Keeffe, M.; Yaghi, O. M. *Science* **2003**, *300*, 1127–1129. (b) Rowsell, J. L.; Millward, A. R.; Park, K. S.; Yaghi, O. M. *J. Am. Chem. Soc.* **2004**, *126*, 5666–5667.
(10) (a) Férey, G.; Latroche, M.; Serre, C.; Millange, F.; Loiseau, T.; Percheron-Guegan, A. *Chem. Commun.* **2003**, 2976–2977. (b) Dybtsev, D. N.; Chun, H.; Kim, K. *Angew. Chem., Int. Ed.* **2004**, *43*, 5033–5036. (c) Zhao, X.; Xiao, B.; Fletcher, A. J.; Thomas, K. M.; Bradshaw, D.; Rosseinsky, M. J. *Science* **2004**, *306*, 1012–1015. (d) Dybtsev, D. N.; Chun, H.; Yoon, S. H.; Kim, D.; Kim, K. *J. Am. Chem. Soc.* **2004**, *126*, 32–33. (e) Pan, L.; Sander, M. B.; Huang, X.; Li, J.; Smith, M.; Bittner, E.; Bockrath, B.; Johnson, J. K. *J. Am. Chem. Soc.* **2004**, *126*, 1308–1309. (f) Lee, E. Y.; Suh, M. P. *Angew. Chem., Int. Ed.* **2004**, *43*, 2798–2801 (g) Kesanli, B.; Cui, Y.; Smith, M. R.; Bittner, E. W.; Bockrath, B. C.; Lin, W. *Angew. Chem., Int. Ed.* **2005**, *44*, 72–75. (h) Kubota, Y.; Takata, M.; Matsuda, R.; Kitaura, R.; Kitagawa, S.; Kato, K.; Sakata, M.; Kobayashi, T. C. *Angew. Chem., Int. Ed.* **2005**, *44*, 920–923. (i) Chen, B.; Ockwig, N. W.; Millward, A. R.; Contreras, D. S.; Yaghi, O. M. *Angew. Chem., Int. Ed.* **2005**, *44*, 4745–4749. (j) Chun, H.; Dybtsev, D. N.; Kim, H.; Kim, K. *Chem.–Eur. J.* **2005**, *11*, 3521–3529. (k) Férey, G.; Mellot-Draznieks, C.; Serre, C.; Millange, F.; Dutour, J.; Surblé, S.; Margiolaki, I. *Science* **2005**, *309*, 2040–2042.
(11) Navarro, J. A. R.; Barea, E.; Salas, J. M.; Masciocchi, N.; Galli, S.; Sironi, A.; Conchi, O. A.; Parra, J. B. *Inorg. Chem.* **2006**, *45*, 2397–2399.
(12) Bhatia, S. K.; Myers, A. L. *Langmuir* **2006**, *22*, 1688–1700.
(13) Mehrotra, R. C.; Bohra, R. *Metal Carboxylates*; Academic Press: London, 1983.
(14) Species of formula Co₄O(O₂C–R)₆ have been identified by mass spectrometry but have not yet been structurally characterized.
(15) (a) Ehlert, M. K.; Rettig, S. J.; Storr, A.; Thompson, R. C.; Trotter, J. *Acta Crystallogr.* **1994**, *C50*, 1023–1026. (b) Mösch-Zanetti, N. C.; Ferbinteanu, M.; Magull, J. *Eur. J. Inorg. Chem.* **2002**, 950–956.
(16) Herr, R. J. *J. Bioorg. Med. Chem.* **2002**, *10*, 3379–3393.

was sealed and heated in a tube furnace at 120 °C for 1 day and allowed to cool to room temperature. Amber, block-shaped crystals suitable for X-ray analysis were collected to give 10 mg (8%) of product. Anal. Calcd for $C_{46}H_{74}Cl_2Mn_3O_6N_{22}$: C, 43.61; H, 5.89; N, 24.32. Found: C, 43.77; H, 6.37; N, 23.85. IR (neat): 2977(w), 2935(w), 2886(w), 1658(s), 1639(vs), 1430(m), 1376(m), 1361(m), 1303(w), 1268(w), 1212(w), 1154(w), 1127(w), 1102(w), 1011(w), 947(w), 861(w), 820-(w), 754(w) cm^{-1}.

Mn$_4$(BDT)$_3$(NO$_3$)$_2$(DEF)$_6$ (2). A solution of Mn(NO$_3$)$_2$·4H$_2$O (25 mg, 0.10 mmol) in 2 mL of DEF was added to a solution of H$_2$BDT (21 mg, 0.10 mmol) in 2 mL of DEF in a Pyrex tube (1.0 × 1.2 × 16 cm, i.d. × o.d. × length), and the mixture was degassed by five freeze−pump−thaw cycles. The tube was sealed and heated in a tube furnace at 130 °C for 2 days and allowed to cool to room temperature. Amber, block-shaped single crystals (2 mg, 3%) were isolated mechanically from the major product, an unidentified amorphous white solid. IR (neat): 3230(b), 2934(b), 2429(b), 2323(b), 1920(b), 1627(vs), 1439-(m), 1389(w), 1359(w), 1271(w), 1212(w), 1159(w), 1133(w), 1036-(w), 1007(w), 833(w), 739(w), 695(w) cm^{-1}.

Zn$_3$(BDT)$_3$(DMF)$_4$(H$_2$O)$_2$·3.5CH$_3$OH (3). A solution of Zn(NO$_3$)$_2$·6H$_2$O (200 mg, 0.66 mmol) in 10 mL of methanol was added to a solution of H$_2$BDT (70 mg, 0.33 mmol) in 10 mL of DMF, and the mixture was allowed to stand at room temperature for 4 days. Color-less, block-shaped crystals were collected by filtration, washed with successive aliquots of DMF (20 mL) and Et$_2$O (20 mL), and dried in air to afford 75 mg (51%) of product. IR (neat): 1648(vs, C=O), 1499(w), 1432(s), 1385(m), 1250(w), 1191(w), 1108(w), 1063(w), 1007(w), 853(w), 749(w), 664(w) cm^{-1}. Anal. Calcd for $C_{39.5}H_{58}$-N$_{28}O_{9.5}$Zn$_3$: C, 37.26; H, 4.59; N, 30.80. Found: C, 37.21; H, 4.91; N, 30.52.

Mn$_3$(BDT)$_3$(DMF)$_4$(H$_2$O)$_2$·3CH$_3$OH·2H$_2$O·DMF (4). A solution of Mn(NO$_3$)$_2$·4H$_2$O (250 mg, 1.0 mmol) in 5 mL of methanol was added to a solution of H$_2$BDT (71 mg, 0.33 mmol) in 5 mL of DMF. Ethyl acetate vapor was diffused into the mixture at room temperature over a period of 2 days. Colorless, block-shaped single crystals were collected by filtration and dried in air to afford 98 mg (66%) of product. IR (neat): 1652(vs, C=O), 1498(w), 1428(s), 1384(m), 1251(w), 1227-(w), 1179(w), 1107(w), 1059(w), 1007(w), 857(w), 748(m), 683(m) cm^{-1}. Anal. Calcd for $C_{42}H_{67}Mn_3N_{29}O_{12}$: C, 37.79; H, 5.06; N, 30.43. Found: C, 38.01; H, 5.22; N: 30.29.

Mn$_2$(BDT)Cl$_2$(DMF)$_2$·1.5CH$_3$OH·H$_2$O (5). A solution of MnCl$_2$·4H$_2$O (200 mg, 1.0 mmol) in 5 mL of methanol was added to a solution of H$_2$BDT (43 mg, 0.20 mmol) in 5 mL of DMF, and the mixture was heated at 70 °C in a Teflon-capped scintillation vial. Off-white, rod-shaped crystals formed after 1 day and were collected by filtration, washed with DMF (20 mL), and dried in air to afford 81 mg (70%) of product. IR (neat): 1646 (vs, C=O), 1494(w), 1431(m), 1386(m), 1252-(w), 1168(w), 1106(m), 1056(m), 1010(m), 857(m), 752(m), 681(m) cm^{-1}. Anal. Calcd for $C_{15.5}H_{26}Mn_2N_{10}O_{4.5}$: C, 30.76; H, 4.33; N, 23.14. Found: C, 30.68; H, 4.72; N, 22.78.

Cu(BDT)(DMF)·CH$_3$OH·0.25DMF (6). A solution of Cu(NO$_3$)$_2$·2.5H$_2$O (93 mg, 0.40 mmol) in 5 mL of methanol was added to a solution of H$_2$BDT (86 mg, 0.37 mmol) in 5 mL of DMF. An aqueous solution of HCl (0.3 mL, 1 M) was added dropwise to the mixture while stirring, affording a clear, bright-green solution. The mixture was

allowed to stand at room temperature for 5 days. The resulting blue, block-shaped crystals were collected to afford 110 mg (71%) of product. IR (neat): 3454(b), 2930(w), 2872(w), 1656(vs), 1494(w), 1433(w), 1406(w), 1389(m), 1251(w), 1095(m), 1063(w), 1030(w), 1004(w), 852-(w), 739(w), 663(w) cm^{-1}. Anal. Calcd for $C_{12.75}H_{16.75}CuN_{9.25}O_{2.25}$: C, 38.37; H, 4.23; N, 32.46. Found: C, 38.38; H, 4.60; N, 32.23.

Gas Sorption Measurements. All gas sorption isotherms were measured using a Micromeritics ASAP2020 volumetric gas adsorption instrument. As-synthesized compounds **3**−**6** were transferred to pre-weighed analysis tubes, which were capped with a Transeal to prevent intrusion of oxygen and atmospheric moisture during transfers and weighing. The samples were evacuated under dynamic vacuum up to 160 °C until the outgas rate was less than 2 mTorr/min. The length of time between the onset of the final temperature and the onset of the 2mTorr/min outgas rate was at least 2 days for all samples, much longer than the temperature ramping time, such that the overall heating and degassing time was approximately the same in all cases, regardless of the heating rate. The evacuated analysis tubes containing degassed samples were then transferred carefully to an electronic balance and weighed to determine the mass of sample. After determining the mass of the degassed samples, the analysis tube was transferred back to the analysis port of the gas adsorption instrument. The outgas rate was again confirmed to be less than 2 mTorr/min. For all isotherms, warm and cold free space correction measurements were effected using ultrahigh purity He gas (UHP grade 5.0, 99.999% purity); H$_2$, N$_2$, and O$_2$ isotherms at 77 K were measured in liquid nitrogen baths using UHP grade gas sources. H$_2$ isotherms at 87 K were measured in liquid argon baths. Oil-free vacuum pumps and oil-free pressure regulators were used for all measurements to prevent contamination of the samples during the evacuation process, or of the feed gases during the isotherm measurement.

X-ray Structure Determinations. Single crystals of compounds **1** and **3**−**5** were coated with Paratone-N oil and mounted on Kapton loops. The crystals were then quickly transferred to a Siemens SMART or Bruker APEX diffractometer, and cooled in a stream of nitrogen gas. Single crystals of compounds **2** and **6** were treated similarly and transferred to a Bruker Platinum 200 Instrument at the Advanced Light Source at the Lawrence Berkeley National Laboratory. Preliminary cell data were collected giving unit cells consistent with the triclinic Laue group for compounds **2**−**4**, and with the monoclinic, orthorhombic, and hexagonal Laue groups for compounds **1**, **6**, and **5**, respectively. The unit cell parameters were later refined against all data. A full hemisphere of data was collected for all compounds. None of the crystals showed significant decay during data collection. Data were integrated and corrected for Lorentz and polarization effects using SAINT 7.07b and were corrected for absorption effects using SADABS 2.10. Crystal and refinement parameters are listed in Table 1.

Space group assignments were based upon systematic absences, E statistics, and successful refinement of the structures. Structures were solved by direct methods and expanded through successive difference Fourier maps. They were refined against all data using the SHELXTL 5.0 software package. Thermal parameters for all non-hydrogen atoms pertaining to the framework skeleton were refined anisotropically in all compounds. Thermal parameters for partially occupied sites associated with disordered C, N, and O atoms pertaining to solvent molecules were refined isotropically. Hydrogen atoms associated with disordered atoms were not included in the structural refinements. All other hydrogen atoms were assigned to ideal positions and refined using a riding model with an isotropic thermal parameter 1.2 times that of the attached atom (1.5 times for methyl hydrogens). The high residual factors obtained in refining the structure of **2** are a consequence of the extreme thermal motion of the ethyl groups pertaining to bound DEF molecules and poor crystal quality due to partial loss of lattice solvent. Due to disorder, the C−N distances in three DEF molecules in the structure of **2** were constrained to idealized lengths of 1.54 Å. Nitrate anions in the structure of **2** could not be located in the residual electron

(17) (a) Carlucci, L.; Ciani, G.; Proserpio, D. M. *Angew. Chem., Int. Ed.* **1999**, *38*, 3488−3492. (b) van Koningsbruggen, P. J.; Garcia, Y.; Kooijman, H.; Spek, A. L.; Haasnoot, J. G.; Kahn, O.; Linares, J.; Codjovi, E.; Varret, F. *J. Chem. Soc., Dalton Trans.* **2001**, 466−471. (c) Grunert, M.; Mills, A. M.; Spek, A. L.; Haasnoot, J. G.; Reedijk, J.; Linert, W. *Dalton* **2003**, 3628−3633. (d) Tao, J.; Ma, Z.-J.; Huang, R.-B.; Zheng, L.-S. *Inorg. Chem.* **2004**, *43*, 6133−6135. (e) Jiang, C.; Yu, Z.; Jiao, C.; Wang, S.; Li, J.; Wang, Z.; Cui, Y. *Eur. J. Inorg. Chem.* **2004**, 4669−4674. (f) Jiang, C.; Yu, Z.; Wang, S.; Jiao, C.; Li, J.; Wang, Z.; Cui, Y. *Eur. J. Inorg. Chem.* **2004**, 3662−3667. (g) Luo, T. T.; Tsai, H. L.; Yang, S. L.; Liu, Y. H.; Dayal Yadav, R. D.; Su, C. C.; Ueng, C. H.; Lin, L. G.; Lu, K. L. *Angew. Chem., Int. Ed.* **2005**, *44*, 6063−6067. (h) Wang, X. S.; Tang, Y. Z.; Huang, X. F.; Qu, Z. R.; Che, C. M.; Chan, P. W. H.; Xiong, R. G. *Inorg. Chem.* **2005**, *44*, 5278−5285.

Table 1. Crystallographic Data^a for Mn$_3$(BDT)$_2$Cl$_2$((DEF)$_6$ (**1**), Mn$_4$(BDT)$_3$(NO$_3$)$_2$((DEF)$_6$ (**2**), Zn$_3$(BDT)$_3$(DMF)$_4$(H$_2$O)$_2$ (**3**), Mn$_3$(BDT)$_3$(DMF)$_4$(H$_2$O)$_2$ (**4**), Mn$_2$(BDT$_8$)Cl$_2$(DMF)$_2$ (**5**), and Cu(BDT)(DMF) (**6**)

	1	2	3	4	5	6
formula	C$_{46}$H$_8$Cl$_2$Mn$_3$N$_{24}$O$_{12}$	C$_{84}$H$_{12}$Mn$_4$N$_{36}$O$_{15}$	C$_{40}$H$_{55}$N$_{29}$O$_8$Zn$_3$	C$_{39}$H$_{12}$Mn$_3$N$_{29}$O$_{10}$	C$_{20.4}$H$_6$Cl$_3$Mn$_3$N$_{14.4}$O$_{13.32}$	C$_{23}$H$_8$Cu$_2$N$_{18}$O$_8$
FW	1324.48	1985.06	1266.24	1211.6	234.19	791.55
T, K	114	173	160	159	176	173
space group	C2/m	P1̄	P1̄	P1̄	R3̄	Imma
Z	2	1	1	1	6	2
a, Å	20.353(13)	10.491(3)	11.571(2)	11.693(3)	33.018(7)	22.340(4)
b, Å	14.477(9)	16.446(5)	11.736(2)	11.994(5)		7.079(1)
c, Å	12.291(8)	19.412(7)	13.619(2)	13.753(3)	8.603(1)	13.644(3)
α, deg		74.64(1)	92.87(1)	92.97(3)		
β, deg	115.30(1)	82.81(1)	114.44(1)	114.36(2)		
γ, deg		78.35(1)	107.99(2)	108.35(2)		
V, Å^3	3274(3)	3153.8(18)	1567.4(5)	1630.5(8)	8123(3)	2157.6(7)
d$_{calc}$, g/cm^3	1.343	1.045	1.342	1.234	1.149	1.218
R$_1$ (wR$_2$), %^{b}	8.36 (22.68)	14.07(33.73)	6.84(20.28)	8.51(25.19)	5.82(14.67)	6.13(18.85)

^{a} Obtained with graphite-monochromated Mo Kα (λ = 0.71073 Å) radiation for **2**, **3**, **4**, and **5**, and synchrotron radiation (λ = 0.775 Å) for **1** and **6**. ^{b} R$_1$ = $\Sigma||F_o| - |F_c||/\Sigma|F_o|$, wR$_2$ = $\{\Sigma[w(F_o^2 - F_c^2)^2]/\Sigma[w(F_o^2)^2]\}^{1/2}$.

density map and were inferred based on charge balance considerations. The structure of **5** was twinned and was best refined by introducing the twin law TWIN 0 1 0 1 0 0 0 0 0−1 in the SHELX instruction file.

Other Physical Measurements. Infrared spectra were collected on a Nicolet Avatar 360 FTIR spectrometer with an attenuated total reflectance accessory (ATR). Carbon, hydrogen, and nitrogen analyses were obtained from the Microanalytical Laboratory of the University of California, Berkeley. Powder X-ray diffraction data was collected using Cu Kα (λ = 1.5406 Å) radiation on a Siemens D5000 diffractometer. Thermogravimetric analyses were carried out at a ramp rate of 1 °C/min in a dinitrogen flow with a TA Instruments TGA 2950.

Results and Discussion

The ligand BDT^{2-} offers a very rich coordination chemistry as a result of having two tetrazolate rings, each with four possible donor nitrogen atoms. Thus, the numerous binding modes of tetrazolate can be expected to give rise to materials with drastically differing structures and gas sorption properties. Indeed, changes in metal counteranion, solvent, and reaction conditions were all found to influence the topology and stability of the resulting frameworks.

Two-Dimensional Frameworks. The reaction between MnCl$_2$·4H$_2$O and H$_2$BDT in DEF at 120 °C in the absence of air afforded Mn$_3$(BDT)$_2$Cl$_2$(DEF)$_6$ (**1**) as amber, block-shaped crystals. If the same reaction is carried out in the air, the initially colorless reaction mixture becomes brown within hours, presumably due to the formation of Mn^{3+} and Mn^{4+} species, and an unidentified brown solid is formed. Instead, if the temperature is maintained below 70 °C, the reaction mixture remains colorless, but only amorphous white powders are formed. Single crystals of **1** are stable outside of the mother liquor for only short periods, after which they gradually become opaque and lose diffraction intensity.

X-ray analysis of a single crystal of **1** revealed a structure in which linear Mn$_3$ units are linked via four BDT^{2-} ligands to produce a neutral two-dimensional framework (see Figure 2). The Mn$_3$ units consist of a central Mn^{2+} ion, octahedrally coordinated by four tetrazolate nitrogen atoms, two trans-oriented bridging chloride anions, and two outer Mn^{2+} ions, each octahedrally coordinated by two tetrazolate nitrogen atoms, one bridging chloride anion, and three DEF molecules. Each tetrazolate ring is attached to two Mn^{2+} ions via its N1 and N2 atoms, a "side-on" coordination mode that is quite uncommon for a tetrazolate ligand.[18] Each trinuclear unit is connected to
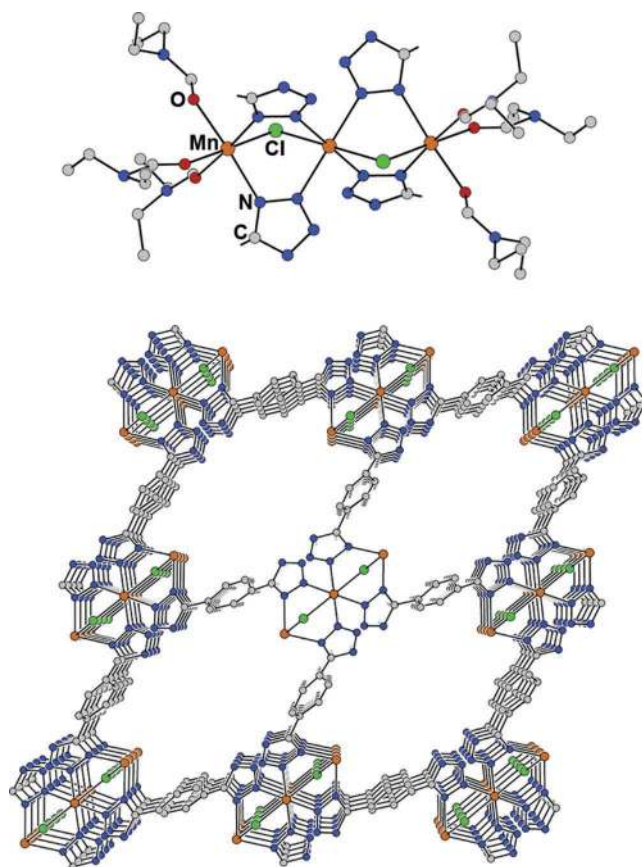

Figure 2. Portions of the crystal structure of **1**, showing the linear Mn$_3$ unit (upper) and, upon removing the DEF molecules, the arrangement of channels along the [001] direction (lower). Hydrogen atoms are omitted for clarity. Selected mean interatomic distances (Å) and angles (deg): Mn−Cl, 2.51(5); Mn−O, 2.18(3); Mn−N, 2.26(2); Mn···Mn, 3.636; Cl−Mn−N, 91(3); Mn−N−N, 120(6); Mn−Cl−Mn, 92.64.

four neighboring clusters and can thus be considered a four-connected node, which together with linear BDT^{2-} edges define a 4,4 plane net.[3] Trinuclear moieties of this type were previously unknown for tetrazoles and are rare among other azoles, with Cu^{2+}- and Cd^{2+}-based triazolate clusters representing the only known examples.[19] Although the layers within **1** stack along

(18) (a) Palopoli, S. F.; Geib, S. J.; Rheingold, A. L.; Brill, T. B. *Inorg. Chem.* **1988**, *27*, 2963−2971. (b) Bhandari, S.; Mahon, M. F.; Molloy, K. C.; Palmer, J. S.; Sayers, S. F. *J. Chem. Soc., Dalton Trans.* **2000**, 1053−1060.
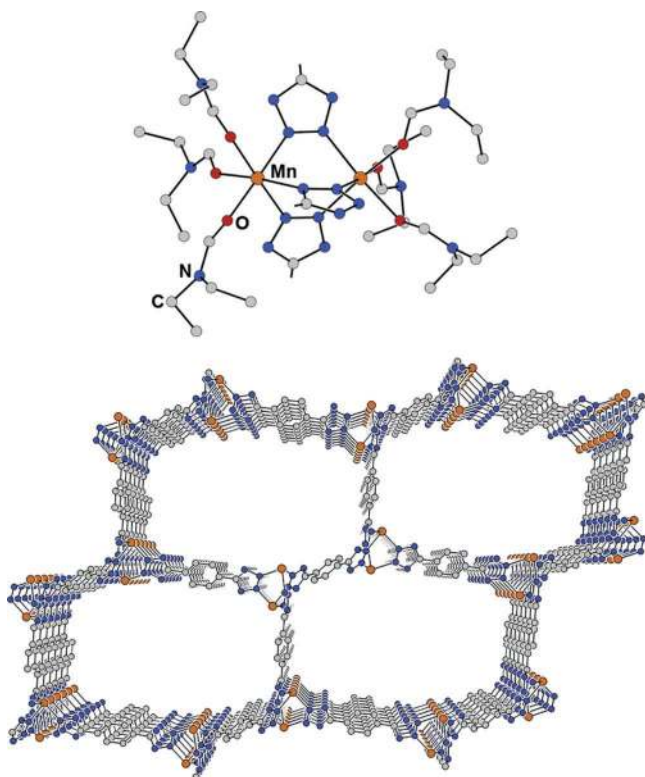
Figure 3. Portions of the crystal structure of **2**, showing the three-bladed paddlewheel building unit (upper), and upon removing the DEF molecules, the disposition of channels along the [100] direction (lower). Hydrogen atoms are omitted for clarity. Selected mean interatomic distances (Å) and angles (deg): Mn−O, 2.17(2); Mn−N, 2.27(2); Mn···Mn, 3.973; N−Mn−N, 89(3); O−Mn−O, 89(2); Mn−N−N, 126(6).

the [001] direction of the crystal to give DEF-filled channels, it is likely that the two-dimensional connectivity leads to framework collapse upon evacuation of the solvent molecules.

In a similar reaction, heating $Mn(NO_3)_2 \cdot 4H_2O$ and H_2BDT in DEF at 130 °C produced a small amount of amber, block-shaped crystals of $[Mn_4(BDT)_3(DEF)_6](NO_3)_2$ (**2**). Crystals of **2** are also stable outside the mother liquor for only short periods, after which loss of crystallinity occurs, evidenced by pronounced loss of X-ray diffraction intensity. X-ray analysis revealed an extended two-dimensional structure containing Mn_2 paddlewheel units in which the metals are connected by three BDT^{2-} ligands via two nitrogen atoms on each tetrazolate ring (see Figure 3). Notably, two tetrazolate coordination modes are present in this structure: two of the tetrazolate rings are coordinated via the N2 and N3 atoms, the more common binding mode, whereas the third ring bridges the two Mn^{2+} ions via the N1 and N2 atoms. Each Mn^{2+} ion has an octahedral coordination geometry, facially coordinated by three N atoms from BDT^{2-} ligands and three oxygen atoms from bound DEF molecules. Although four-bladed paddlewheel units are ubiquitous among carboxylate-based molecular species[2,13] and metal−organic frameworks,[20] this represents the first example of a metal−organic framework based on a three-bladed paddlewheel unit. A geometrically related dinuclear unit is found, however, in $[Mn_2(CO)_6(N_4C−$

$R)_3]^-$ ($R = CF_3, F_2NCF_2$),[21] Mn^I-containing compounds which, to our knowledge, are the only molecular analogues of the Mn_2 paddlewheel units observed in **2**. If the paddlewheel units in **2** are regarded as three-connected nodes, then linear BDT^{2-} bridging ligands function as edges of a 6,3 plane net,[3] also known as the honeycomb structure. Stacking of the two-dimensional sheets affords hexagonal one-dimensional channels in which disordered nitrate anions and unbound solvent molecules reside. Again, degradation of **2** outside the mother liquor is probably due to collapse of the loosely connected two-dimensional framework, which is unlikely to sustain porosity upon desolvation.

Three-Dimensional Frameworks. Exploration of the coordination chemistry of a given ligand involves systematic variation of several reaction parameters, among which the solvent mixture typically plays an important role. We found that reactions run in neat DMF or dimethyl sulfoxide produced either unidentified crystalline powders or amorphous precipitates regardless of temperature or concentration. Because the poor solubility of H_2BDT in other organic solvents or water limited the choice of solvent, solvent mixtures were employed for this system. We found that replacement of DEF with an equimolar mixture of methanol and DMF increases the dimensionality of the ensuing frameworks, promoting formation of microporous solids. For example, the reaction between $Zn(NO_3)_2 \cdot 6H_2O$ and H_2BDT in this solvent mixture produces large, colorless crystals of $Zn_3(BDT)_3(DMF)_4(H_2O)_2 \cdot 3.5CH_3OH$ (**3**) upon sitting for several days at room temperature. Increasing the reaction temperature interferes with the crystallization process, because poorly crystalline powders are formed in only a few hours at higher temperature. An analogue of **3**, $Mn_3(BDT)_3(DMF)_4-(H_2O)_2 \cdot 3CH_3OH \cdot 2H_2O \cdot DMF$ (**4**), can be synthesized under similar conditions starting from $Mn(NO_3)_2 \cdot 4H_2O$. In this case, however, diffusion of ethyl acetate vapor into the reaction solution is necessary to induce crystallization, suggesting that the Mn^{2+}-containing framework is somewhat more soluble in the polar solvent mixture.

X-ray analysis of single crystals of **3** and **4** showed the two compounds to be isomorphous, crystallizing in the same space group and exhibiting virtually identical unit cell parameters (see Table 1). Their structures contain linear M_3 (M = Mn, Zn) units linked via BDT^{2-} bridges to form a neutral, three-dimensional framework (see Figure 4). The M_3 units consist of a central M^{2+} ion coordinated octahedrally by six tetrazolate nitrogen atoms and two outer M^{2+} ions, each coordinated by three tetrazolate nitrogen atoms, two DMF molecules, and one water molecule in an almost ideal octahedral geometry. Note that trinuclear moieties of this type are currently unknown for tetrazolates but that discrete molecular species of the type $M_3-(tz)_6(H_2O)_6$ (M = Mn, Fe, Co, Ni, Cu, Zn; tz = 4-substituted 1,2,4-triazoles) have been isolated.[22] In **3** and **4**, the M_3 units stack along one direction such that, together with the bridging BDT^{2-} ligands, they define one-dimensional channels in which

(19) (a) van Koningsbruggen, P. J.; van Hal, J. W.; de Graaff, R. A. G.; Haasnoot, J. G.; Reedijk, J. *J. Chem. Soc., Dalton Trans.* **1993**, 2163-2167. (b) Prins, R.; Biagini-Cingi, M.; Drillon, M.; de Graaff, R. A. G.; Haasnoot, J.; Manotti-Lanfredi, A.-M.; Rabu, P.; Reedijk, J.; Ugozzoli, F. *Inorg. Chim. Acta* **1996**, *248*, 35−44. (c) Yi, L.; Ding, B.; Zhao, B.; Cheng, P.; Liao, D.-Z.; Yan, S.-P.; Jiang, Z.-H. *Inorg. Chem.* **2004**, *43*, 33−43.

(20) (a) Li, H.; Eddaoudi, M.; Groy, T. L.; Yaghi, O. M. *J. Am. Chem. Soc.* **1998**, *120*, 8571−8572. (b) Reineke, T. M.; Eddaoudi, M.; Moler, D.; O'Keeffe, M.; Yaghi, O. M. *J. Am. Chem. Soc.* **2000**, *122*, 4843−4844. (c) Chen, B.; Eddaoudi, M.; Reineke, T. M.; Kampf, J. W.; O'Keeffe, M.; Yaghi, O. M. *J. Am. Chem. Soc.* **2000**, *122*, 11559−11560. (d) Chen, B.; Eddaoudi, M.; Hyde, S. T.; O'Keeffe, M.; Yaghi, O. M. *Science* **2001**, *291*, 1021−1023.

(21) John, E. O.; Willett, R. D.; Scott, B.; Kirchmeier, R. L.; Shreeve, J. M. *Inorg. Chem.* **1989**, *28*, 893−897.
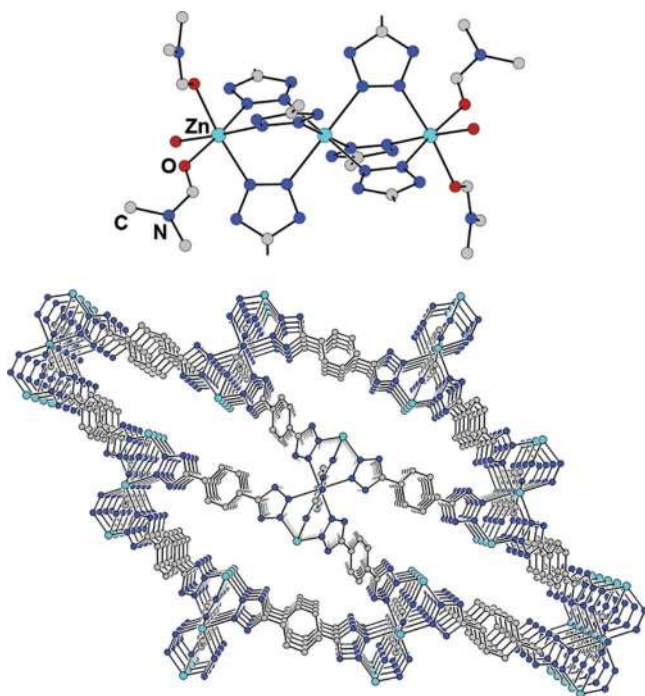
Figure 4. Portions of the crystal structure of **3**, showing the trinuclear Zn₃ building units (upper) and, upon removing the DMF and water ligands, the arrangement of channels along the [001] direction. Hydrogen atoms and solvate guest molecules are omitted for clarity. Selected mean interatomic distances (Å) and angles (deg) from the isotypic structures of **3** (M = Zn) and **4** (M = Mn), respectively: M−O, 2.08(4), 2.15(4); M−N, 2.15(3), 2.25(2); M···M, 3.763, 3.951; N−M-N, 90(3), 89(3); O−M-O, 90(2), 90-(2); M−N−N, 125(3), 125(2).

DMF, water, and disordered methanol molecules reside. The trinuclear moieties and the linear BDT²⁻ ligands in **3** and **4** can be viewed as the six-connected nodes and edges of a 4,6 three-dimensional net, respectively.[3] The simplified structures of **3** and **4** thus have the same connectivity but lower symmetry than a primitive cubic net. These structures are isomorphous with another recently reported BDT²⁻-containing framework, Cd₃(BDT)₃(DMF)₄(H₂O)₂,[17d] and have the same connectivity as a series of dicarboxylate-based frameworks: Zn₃(BDC)₃(CH₃-OH)₄·2CH₃OH,[23] Mg₃(NDC)₃(DEF)₄ (NDC = 2,6-naphthalenedicarboxylate),[24] Zn₃(NDC)₃(CH₃OH)₂·2DMF·H₂O,[24] and Ni₃(NDC)₃(NC₅H₅)₄.[25] Importantly, the comparison of **3** with Zn₃(BDC)₃(CH₃OH)₄·2CH₃OH demonstrates for the first time that 1,4-benzeneditetrazolate is indeed capable of forming direct structural analogues of metal−organic frameworks incorporating 1,4-benzenedicarboxylate.

When MnCl₂·4H₂O is employed in place of Mn(NO₃)₂·4H₂O, the reaction with H₂BDT yields a new three-dimensional framework structure type. Upon heating the reaction solution at 70 °C for 1 day, colorless hexagonal rod-shaped crystals of Mn₂(BDT)Cl₂(DMF)₂·1.5CH₃OH·H₂O (**5**) formed. As was also
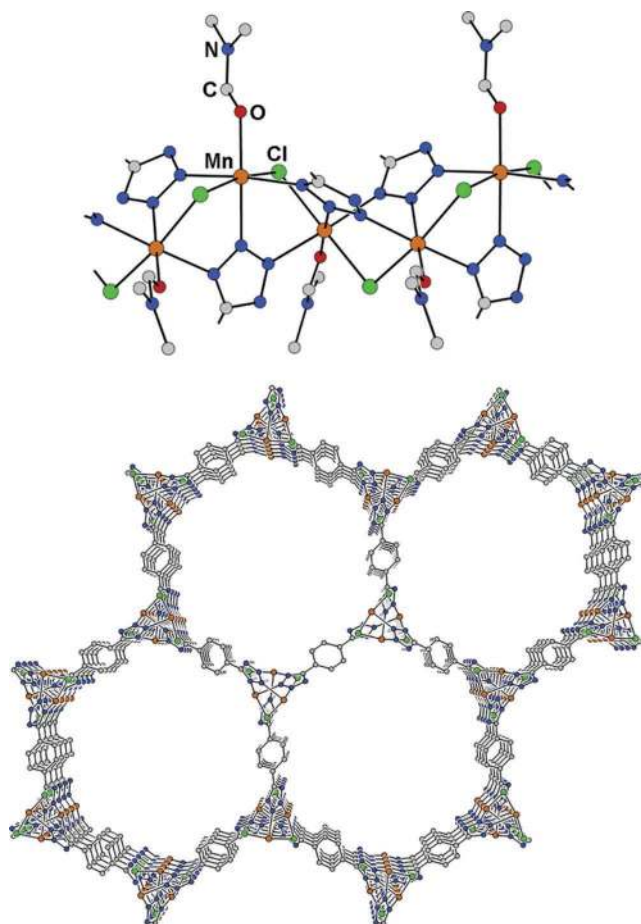
(22) Representative examples: (a) Vos, G.; Haasnoot, J. G.; Verschoor, G. C.; Reedijk, J.; Schaminee, P. E. L. *Inorg. Chim. Acta* **1985**, *105*, 31−39. (b) Vos, G.; Le Febre, R. A.; de Graaff, R. A. G.; Haasnoot, J. G.; Reedijk, J. *J. Am. Chem. Soc.* **1983**, *105*, 1682−1683. (c) Antolini, L.; Fabretti, D.; Gatteschi, D.; Giusti, A.; Sessoli, R. *Inorg. Chem.* **1991**, *30*, 4858−4860. (d) Vreugdenhil, W.; Haasnoot, J. G.; Reedijk, J. R.; Wood, J. S. *Inorg. Chim. Acta* **1990**, *167*, 109−113. (e) Liu, J.; Song, Y.; Yu, Z.; Zhuang, J.; Huang, X.; You, X. *Polyhedron* **1999**, *18*, 1491−1494. (f) Spek, A. L.; Vos, G. *Acta Crystallogr.* **1983**, *C39*, 990−993.
(23) Li, H.; Davis, C. E.; Groy, T. L.; Kelley, D. G.; Yaghi, O. M. *J. Am. Chem. Soc.* **1998**, *120*, 2186−2187.
(24) Dinca, M.; Long, J. R. *J. Am. Chem. Soc.* **2005**, *127*, 9376−9377.
(25) Kongshaug, K. O.; Fjellvåg, H. *Solid State Sci.* **2003**, *5*, 303−310.

Figure 5. Portions of the crystal structure of **5**, showing part of the infinite helical chains composed of Mn²⁺ and Cl⁻ ions (upper) and, upon removing the DMF molecules, the one-dimensional channels formed along the [001] direction (lower). Hydrogen atoms and guest solvent molecules are also omitted for clarity. Selected mean interatomic distances (Å) and angles (deg): Mn−Cl, 2.51(1); Mn−O, 2.139(1); Mn−N, 2.29(2); Mn···Mn, 3.759-(1); Cl−Mn−N, 88(3); Mn−N−N, 117(19); Mn−Cl−Mn, 93(4).

the case with reactions run in DEF, increasing the reaction temperature led to oxidation of Mn²⁺ such that formation of **5** was accompanied by the formation of unidentified brown powders. In contrast, decreasing the temperature below 60 °C retarded the reaction time by several days, and **5** could only be isolated in lower yield. X-ray analysis of **5** revealed one-dimensional helical chains composed of alternating Mn²⁺ and Cl⁻ ions, which are connected through bridging BDT²⁻ ligands to form a neutral three-dimensional framework (see Figure 5). Each Mn²⁺ ion is coordinated octahedrally by three meridionally arranged tetrazolate nitrogen atoms, two bridging chloride anions situated trans to each other, and a terminal DMF ligand. The structure of **5** can also be described as a three-dimensional net composed of helical chains of opposing chirality, 3₁ and 3₂, linked via linear bridges. As such, **5** can be categorized either as an (8,3)-b net in the notation of Wells,[3,26] or as an *etb*-type net in the notation of O'Keeffe and Yaghi.[27] To our knowledge, this type of net has been encountered previously only within Zn₂(DHBDC)(H₂O)₂·0.5H₂O·1.5C₂H₅OH (DHBDC²⁻ = 2,5-dihydroxy-1,4-benzenedicarboxylate)[27] and

(26) Wells, A. F. *Three-Dimensional Nets and Polyhedra*; Wiley: New York, 1977.
(27) Rosi, N. L.; Kim, J.; Eddaoudi, M.; Chen, B.; O'Keeffe, M.; Yaghi, O. M. *J. Am. Chem. Soc.* **2005**, *127*, 1504−1518.

its analogues, $M_2(DHBDC)(H_2O)_2 \cdot 8H_2O$ (M = Co, Ni).[28] The N1, N2, and N3 atoms of each tetrazolate ring in **5** act as donor ligands to three distinct Mn^{2+} ions, representing a coordination mode previously observed only in the 5-methyltetrazolate-bridged framework of $[Zn(H_3CCN_4)_2](H_2O)_4$.[17h] Significantly, connection of the infinite chains through the BDT^{2-} ligands defines 19.6 Å-wide one-dimensional channels running along the [001] direction of the crystal and filled with bound DMF molecules and guest methanol and water solvate molecules.

Reaction of $Cu(NO_3)_2 \cdot 2.5H_2O$ with H_2BDT in an acidic mixture of DMF and methanol produces a different three-dimensional framework. Notably, if the same reaction is attempted under neutral conditions, only a blue amorphous precipitate is formed. This precipitate dissolves quickly upon addition of aqueous HCl to give a bright green solution from which large deep-blue block-shaped crystals of Cu(BDT)-(DMF)·0.25DMF·CH_3OH (**6**) are deposited after 2 days at room temperature. If the acidic mixture is instead heated above 40 °C, a poorly crystalline blue precipitate is formed within minutes, suggesting that the acidic medium and low temperature are critical for the slow crystallization process that allows the formation of single crystals in this case. X-ray analysis of **6** revealed a structure in which infinite one-dimensional chains of Cu^{2+} ions are linked by BDT^{2-} ligands to form the neutral framework depicted in Figure 6. Each Cu^{2+} ion is coordinated octahedrally by four tetrazolate nitrogen atoms and two trans-oriented bridging DMF molecules. A pronounced Jahn−Teller distortion, common for Cu^{2+} ions, is also evident along the axis containing the two DMF molecules. Indeed, the mean Cu−N bond length of 1.998(1) Å, is considerably shorter than the mean Cu−O bond length of 2.451(1) Å. Bridging DMF molecules, although fairly common in main group[29] and lanthanide metal compounds,[30] are rare in transition metal chemistry, particularly for first-row metal ions.[31] The infinite Cu^{2+} chains, together with the bridging BDT^{2-} ligands, define wide, rhombic one-dimensional channels, running along the [010] direction of the crystal, with diagonal dimensions of 13.6 Å × 22.3 Å. Bound DMF molecules protrude into these channels, with the remaining space taken up by disordered DMF, methanol, and possibly water guest molecules.

Gas Sorption Properties. Typically, two-dimensional frameworks are less likely to exhibit sustainable porosity upon desolvation, presumably due to collapse of the two-dimensional layers and ulterior blocking of potential pores. This, combined with the relatively low yields obtained for compounds **1** and **2**, prompted us to perform gas sorption measurements only on compounds **3**−**6**.

Thermogravimetric analyses of compounds **3**−**5** showed no clear weight loss plateaus, prompting us to investigate their
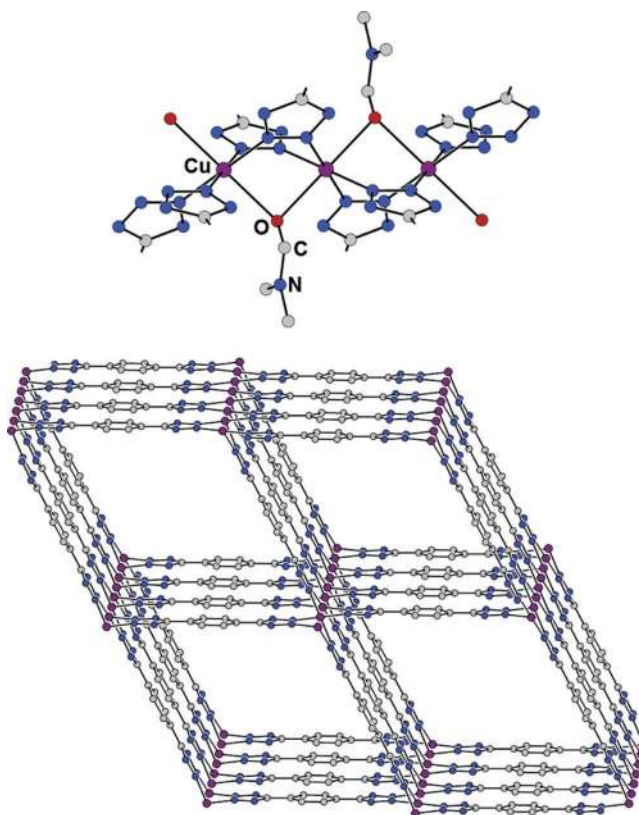

Figure 6. Portions of the crystal structure of **6**, showing part of the one-dimensional Cu^{2+} chains (upper) and, upon removing DMF molecules, the arrangement of one-dimensional layers along the [010] direction (lower). Hydrogen atoms and solvent molecules were omitted for clarity. Selected interatomic distances (Å) and angles (deg): Cu−O, 2.451(1); Cu−N, 1.998-(1); Cu···Cu, 3.539(1); Cu−O−Cu, 92.45(1); N−Cu−N, 89.94(1); O−Cu−N2, 84.63(1); O−Cu−N3, 95.37(1); Cu−N−N, 123.56(1).
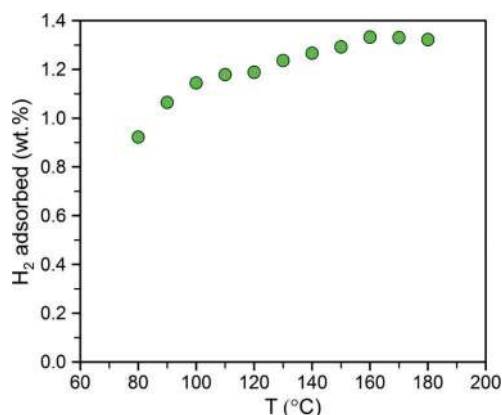

Figure 7. Maximal H_2 uptake in desolvated **3** at 77 K and 900 Torr, after degassing at temperatures between 80 and 180 °C.

stability toward solvent evacuation by means of gas adsorption isotherms. In these cases, to determine the highest possible evacuation temperature before noticeable collapse of the frameworks, samples were heated under dynamic vacuum at increasingly high temperatures, and upon complete degassing, hydrogen adsorption isotherms were measured. Figure 7 shows a series of one-point adsorption measurements corresponding to H_2 uptake in desolvated **3** at 77 K and 900 Torr upon degassing at 10 °C intervals in the range 80−180 °C. During this study, the H_2 uptake increased from 0.92 wt % upon degassing at 80 °C, reaching a maximum of 1.35 wt % after degassing at 160 °C,

(28) (a) Dietzel, P. D. C.; Morita, Y.; Blom, R.; Fjellvåg, H. *Angew. Chem., Int. Ed.* **2005**, *44*, 6354−6358. (b) Dietzel, P. D. C.; Panella, B.; Hirscher, M.; Blom, R.; Fjellvåg, H. *Chem. Commun.* **2006**, 959−961.

(29) (a) Rao, C. P.; Rao, A. M.; Rao, C. N. *Inorg. Chem.* **1984**, *23*, 2080−2085. (b) Rasika Dias, H. V.; Lu, H.-L.; Ratcliff, R. E.; Bott, S. G. *Inorg. Chem.* **1995**, *34*, 1975−1976. (c) Geier, J.; Harmer, J.; Grützmacher, H. *Angew. Chem., Int. Ed.* **2004**, *43*, 4093−4097.

(30) (a) Cunningham, J. A.; Sievers, R. E. *J. Am. Chem. Soc.* **1975**, *97*, 1586−1588. (b) Furphy, B. M.; Harrowfield, J. M.; Kepert, D. L.; Skelton, B. W.; White, A. H.; Wilner, F. R. *Inorg. Chem.* **1987**, *26*, 4231−4236. (c) Harrowfield, J. M.; Ogden, M. I.; White, A. H. *Aust. J. Chem.* **1991**, *44*, 1249−1262.

(31) (a) Psomas, G.; Stemmler, A. J.; Dendrinou-Samara, C.; Bodwin, J. J.; Schneider, M.; Alexiou, M.; Kampf, J. W.; Kessissoglou, D. P.; Pecoraro, V. *Inorg. Chem.* **2001**, *40*, 1562−1570. (b) Kajiwara, T.; Shinagawa, R.; Ito, T.; Kon, N.; Iki, N.; Miyano, S. *Bull. Chem. Soc. Jpn.* **2003**, *76*, 2267−2275.
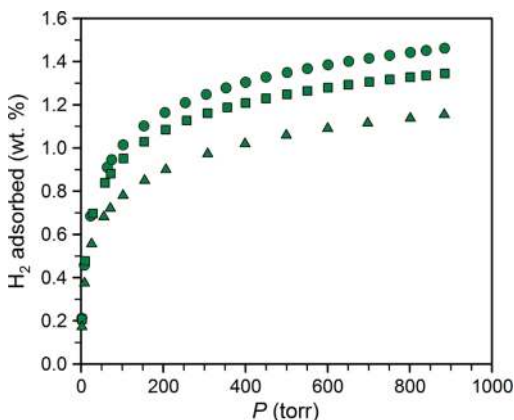
Figure 8. Adsorption isotherms for the H$_2$ uptake in **3** at 77 K upon degassing at 160 °C after heating from 25 to 160 °C via three routes: heating at a rate of 10 °C/min (▲), heating at a rate of 0.1 °C/min (■), and heating at a rate of 0.1 °C/min with four intermediate pauses for complete evacuation (●).

Figure 9. Adsorption isotherms for the H$_2$ uptake in desolvated samples of **3** (dark green circles), **4** (blue circles), and **5** (red circles) at 77 K.

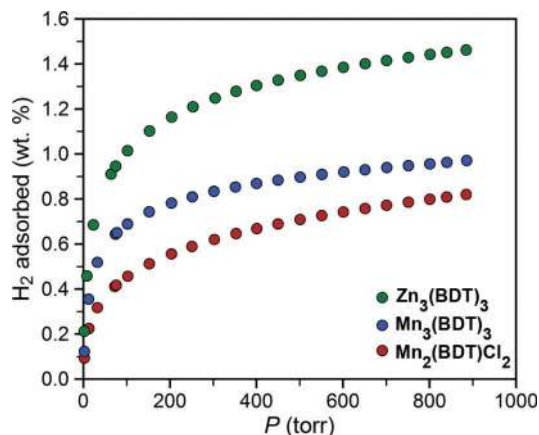**Figure 10.** Adsorption isotherms for the N$_2$ uptake in desolvated samples of **3** (dark green circles), **4** (blue circles), and **5** (red circles) at 77 K and up to 1 atm.

before decreasing slightly to 1.32 wt % after degassing at 180 °C. Similar degassing experiments with **4** and **5** also showed an optimal degassing temperature of 160 °C translated into the highest surface area measurements, and consequently into the highest H$_2$ adsorption capacities.[32] We therefore infer that incomplete activation and partial collapse of the frameworks are responsible for the lower adsorption capacities observed upon degassing below or above 160 °C. Indeed, the decomposition of the frameworks at temperatures above 160 °C is also evidenced by color changes from white to yellow in all three cases.

In addition to the relationship between degassing temperature and gas uptake, we found that the temperature ramping sequence also plays a major role in the maximum adsorption capacity of the material. As shown in Figure 8, heating **3** from 25 to 160 °C at a rate of 10 °C/min prior to degassing resulted in an H$_2$ uptake of only 1.15 wt %, whereas retarding the heating to a rate of 0.1 °C/min resulted in an uptake of 1.35 wt %. The best results were obtained when slow ramping was also accompanied by complete evacuation (outgas rates of 2 mTorr/min or less) at four equally spaced intermediate temperatures. Use of this very mild evacuation procedure gave a maximum H$_2$ uptake of 1.46 wt % for Zn$_3$(BDT)$_3$ at 77 K and 880 Torr. Samples of **4** and **5** were degassed using the same mild evacuation procedure prior to measurement of gas adsorption isotherms. As shown in Figure 9, the H$_2$ adsorption isotherms at 77 K reveal reversible uptakes of 0.97 and 0.82 wt % at 880 Torr for Mn$_3$(BDT)$_3$ and Mn$_2$(BDT)Cl$_2$, the desolvated forms of **4** and **5**, respectively.

The optimally desolvated materials also adsorb significant amounts of N$_2$. Fitting the BET equation to the N$_2$ adsorption isotherms (see Figure 10) gave estimated surface areas of 640, 290, and 530 m^2/g for Zn$_3$(BDT)$_3$, Mn$_3$(BDT)$_3$, and Mn$_2$(BDT)-Cl$_2$, respectively.[33] Notably, there is a large discrepancy between the adsorption properties of Zn$_3$(BDT)$_3$ and Mn$_3$(BDT)$_3$. Although the structures of **3** and **4** are isotypic, Zn$_3$(BDT)$_3$ adsorbs almost twice as much H$_2$ as Mn$_3$(BDT)$_3$ at 880 Torr
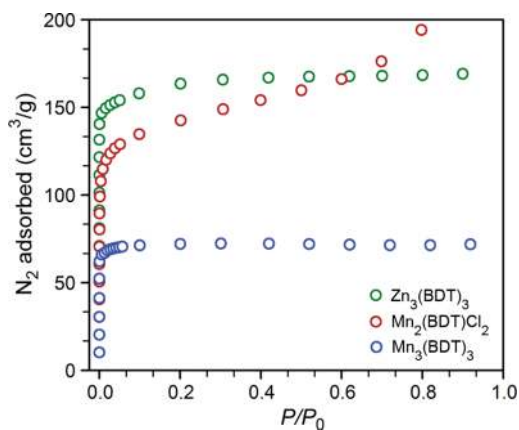
and, consistently, has more than double the surface area of Mn$_3$-(BDT)$_3$. Because identical degassing procedures were used for both compounds, we believe, on the basis of the X-ray crystal structures, that the differences are due to their different response to desolvation. Significantly, the mean Mn−N bond distance in **4**, 2.25(2) Å, is significantly longer than the average Zn−N distance in **3**, 2.15(3) Å. The metal−ligand bonds are likely the weakest links in metal−organic frameworks, and breaking or reorganization of these bonds is what presumably leads to collapse upon desolvation. The longer, weaker Mn−N bonds are therefore probably responsible for the partial collapse, lower surface area, and reduced H$_2$ adsorption capacity of Mn$_3$(BDT)$_3$.

A comparison of the isotherms plotted in Figures 9 and 10 leads to seemingly contradictory H$_2$ and N$_2$ uptake quantities for Mn$_3$(BDT)$_3$ and Mn$_2$(BDT)Cl$_2$. Although Mn$_2$(BDT)Cl$_2$ adsorbs less hydrogen at 880 Torr, its surface area is almost twice that of Mn$_3$(BDT)$_3$. Expectedly, both N$_2$ isotherms rapidly reach saturation at 77 K, whereas neither H$_2$ isotherm is saturated at this temperature. It is obvious from the shapes of the two H$_2$ isotherms, however, that Mn$_3$(BDT)$_3$ is closer to saturation than Mn$_2$(BDT)Cl$_2$ at 1 atm. Accordingly, we can expect that at high-pressure, Mn$_2$(BDT)Cl$_2$ will outperform Mn$_3$-(BDT)$_3$ in terms of H$_2$ uptake, thus agreeing with the observed difference in the N$_2$ adsorption capacities of the two materials.

Although the H$_2$ adsorption capacities of 0.82−1.46 wt % are only average compared to the uptake observed in other

---

(32) Powder X-ray diffraction patterns of the evacuated forms of **3**−**5** showed complete loss of diffraction intensity, indicating loss of long-range ordering but not necessarily loss of porosity, as evidenced by the gas-adsorption experiments.

(33) For comparison, the highest surface area reported for a crystalline zeolite is 904 m^2/g: Chester, A. W.; Clement, P.; Han, S. U.S. Patent 2000/ 6,136,291A.
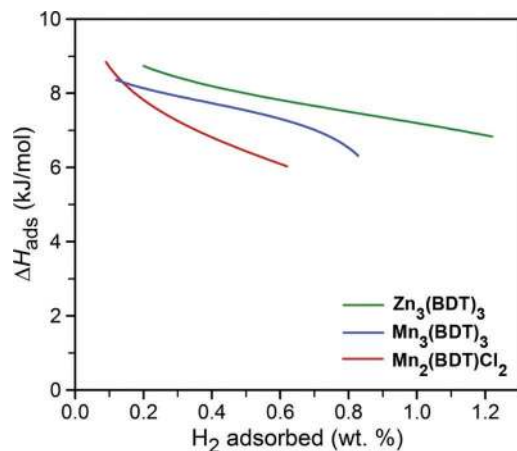
Figure 11. Enthalpy of adsorption plots as a function of the uptake of H_2 in desolvated samples of **3** (dark green), **4** (blue), and **5** (red).

Figure 12. Gas sorption isotherms for the uptake of N_2, H_2, and O_2 in Cu(BDT) at 77 K.

metal−organic framework compounds, the steep initial slope of all three isotherms indicates the presence of strong H_2 adsorption sites inside the pores. The existence of such sites was also anticipated from the X-ray crystal structures of **3**, **4**, and **5**, which suggest that coordinatively unsaturated Zn^{II} and Mn^{II} centers should become accessible upon release of bound DMF and H_2O molecules (see Figures 4 and 5). Consequently, a second set of H_2 isotherms were measured at 87 K and, upon applying a variant of the Clausius−Clapeyron equation, isosteric heats of adsorption were calculated for the three evacuated materials.[24]

As shown in Figure 11, the enthalpies of adsorption lie in the ranges 6.8−8.7 kJ/mol for $Zn_3(BDT)_3$, 6.3−8.4 kJ/mol for $Mn_3(BDT)_3$, and 6.0−8.8 kJ/mol for $Mn_2(BDT)Cl_2$. These values are generally higher than the previously reported H_2 adsorption enthalpies of 4.7−5.2 kJ/mol for $Zn_4O(BDC)_3$,[34,35] 5.3−7.4 kJ/mol in the dehydrated Prussian Blue analogues M_3-$[Co(CN)_6]_2$ (M = Mn, Fe, Co, Ni, Cu, Zn),[34] 5.4−7.3 kJ/mol for silica gel,[36] and 3.9−5.2 kJ/mol for variously functionalized activated carbons.[37] Indeed, these are among the highest values yet reported for metal−organic frameworks. The enthalpies of adsorption observed at low coverage, 8.4−8.8 kJ/mol, are exceeded only by $Mg_3(NDC)_3$ and $Zn_4O(THPDC)_3$ (THPDC = tetrahydropyrenedicarboxylate), which at low coverage show H_2 adsorption enthalpies of 9.5 and 9.1 kJ/mol, respectively. In both cases, however, the high values were attributed to increased van der Waals contact areas associated with small pore sizes. Importantly, the enthalpy plots in Figure 11 also display a significant upward trend at the lowest coverages measured, suggesting that sites with even higher binding enthalpies are actually present in the materials. In view of a recent study indicating an ideal enthalpy change of 15 kJ/mol for H_2 storage at room temperature with pressures in the range 1.5−30 bar,[12] the values reported here represent significant progress toward achieving fully reversible, high-temperature adsorption.

A thermogravimetric analysis of compound **6** showed that it readily releases unbound and most of the bound solvent molecules upon heating under a dinitrogen flow in the range
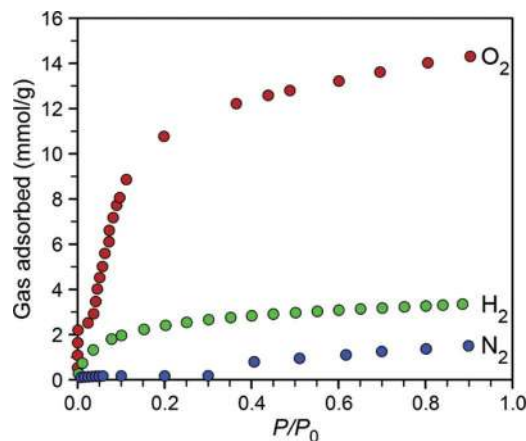
100−210 °C. The observed weight loss of 29% below 210 °C corresponds to release of approximately one methanol and 1.25 DMF molecules per formula unit. To evaluate whether the framework porosity is maintained upon evacuation, a sample of **6** was heated under dynamic vacuum at 160 °C until the outgas rate was less than 2 mTorr/min.[38] During the degassing process, the color of the sample changed from dark blue, to bright green, and then finally to gray, indicating a change in the coordination environment of the Cu^{2+} ions (in agreement with the loss of bound DMF molecules). As such, we can expect the desolvated form of **6**, Cu(BDT), to be a microporous material that exhibits Cu^{2+} centers with unsaturated coordination sites, presumably along the Jahn−Teller distortion axis.

The gas sorption characteristics of Cu(BDT) were therefore also probed via low-temperature isotherm measurements. As shown in Figure 12, the H_2 adsorption isotherm at 77 K reveals a reversible uptake of just 3.3 mmol/g (0.92 mol/mol, 0.66 wt %) at 880 Torr. This represents a lower storage capacity than might be expected from the large one-dimensional channels observed in the crystal structure of **6** (see Figure 6), suggesting that the pores of Cu(BDT) may constrict upon evacuation of the solvent molecules. Although single crystals of **6** lose integrity upon desolvation, preventing structural characterization of Cu-(BDT), the powder X-ray diffraction of Cu(BDT) does not match with that of **6**, suggesting that a significant structural change occurs in **6** upon solvent evacuation. Attempts to measure a BET surface area using N_2 revealed almost no N_2 adsorption at pressures up to 1 atm (see Figure 12), also suggesting a constriction of the pore aperture. Indeed, preferential adsorption of H_2 over N_2 has been observed previously for $Mg_3(NDC)_3$ and $Mn(HCOO)_2$,[10d,24] and has been attributed to a molecular sieving effect associated with the small pore sizes of the desolvated materials.

To estimate the size of the pores in Cu(BDT), an O_2 adsorption isotherm was also measured at 77 K. Note that the kinetic diameter of O_2 (2.46 Å) is slightly smaller than that of N_2 (2.64 Å), and adsorption experiments utilizing gases of varying sizes is a standard means of inferring pore sizes in molecular sieves.[39] To avoid condensation of O_2 at 77 K, which is below its boiling point of 90 K, the saturation pressure was

(34) Kaye, S. S.; Long, J. R. *J. Am. Chem. Soc.* **2005**, *127*, 6506−6507.
(35) Rowsell, J. L. C.; Yaghi, O. M. *J. Am. Chem. Soc.* **2006**, *128*, 1304−1315.
(36) Basmadjian, D. *Can. J. Chem.* **1960**, *38*, 141−148.
(37) Zhao, X. B.; Xiao, B.; Fletcher, A. J.; Thomas, K. M. *J. Phys. Chem. B* **2005**, *109*, 8880−8888.

(38) Degassing at temperatures between 130 and 180 °C resulted in nearly identical adsorption capacities.
(39) Breck, D. W. *Zeolite Molecular Sieves*; Wiley & Sons: New York, 1974.

measured at intervals of 120 min during the experiment. As shown in Figure 12, the sample adsorbed significant amounts of O_2 at 77 K. Unexpectedly, however, the O_2 isotherm revealed two distinct adsorption steps: one in the P/P_0 interval 0−0.025, and the second in the interval 0.025−1. At a relative pressure of 0.025, a first saturation plateau occurs, and the BET equation provides a good fit to this first part of the isotherm to give an estimated surface area of 200 m^2/g.[33] Notably, the monolayer coverages predicted by fitting Langmuir equations to the H_2 and O_2 isotherms are almost identical, (2.56 and 2.53 mmol/g, respectively) and correspond to 0.75 gas molecules/formula unit, suggesting that the same number of binding sites is initially available to both gases. The second, much more significant adsorption step, occurs in the relative pressure interval 0.03−0.2 and corresponds to adsorption of ca. 10 mmol/g of O_2 in excess of what was expected based on the H_2 isotherm. Although hysteresis is observed between the adsorption and desorption curves, O_2 uptake in Cu(BDT) is reversible, suggesting that O_2 does not permanently bind to the framework via an irreversible process such as oxidation of the metal centers.

Stepwise, hysteretic, pressure-dependent gas adsorption of this type has been observed previously in several flexible porous metal−organic frameworks that exhibit "breathing" or "swelling" effects.[40] The unusual gas uptake behavior in these materials has usually been attributed either to favorable adsorbent−adsorbate molecular interactions, such as the adsorption of methanol in desolvated $Cu_2(pzdc)_2(dpyg)\cdot 8H_2O$ (pzdc = pyrazinedicarboxylate, dpyg = 1,2-dipyridylglycol),[40d] or to pressure-dependent gating effects, as observed in the high-pressure adsorption of N_2, O_2, CO_2, and CH_4 in evacuated [Cu-(dhbc)$_2$(4,4′-bpy)]·H$_2$O.[40e] One of these mechanisms is likely in effect here, and high pressure adsorption studies to test this hypothesis are currently underway. Importantly, although Cu-(BDT) is not a promising H_2 storage material at low pressure, its low H_2 and N_2 adsorption capacity of Cu(BDT) and its excellent O_2 uptake at low pressure may be of use for gas separations or purification. Indeed, inspection of the pure component adsorption isotherms of Cu(BDT) and comparisons with those of other molecular sieves suggest that this material should have very high O_2/N_2 and O_2/H_2 selectivity ratios.

Outlook

The foregoing results demonstrate the utility of nitrogen-based heterocyclic ligands, especially tetrazoles, for producing microporous metal−organic frameworks with permanent porosity, and topologies and gas adsorption characteristics mimicking those of carboxylate-based materials. More importantly, these results show that the rich coordination chemistry of tetrazolates can give rise to new structure types that have not yet been accessible using carboxylate chemistry. A thorough investigation of the coordination chemistry of only one ditopic ligand, BDT^{2-}, enabled the synthesis of six porous frameworks, suggesting that judicious design and utilization of related ligands could perhaps produce materials with improved properties. In particular, the new materials disclosed here show the potential of tetrazolate-based ligands for generating frameworks with coordinatively unsaturated metal centers. Such frameworks are of importance to the development of hydrogen storage materials exhibiting enhanced H_2 binding enthalpies, but may also be of interest for applications in catalysis. Accordingly, our future efforts will focus on employing new organoazolate ligands to produce rigid metal−organic frameworks with higher concentrations of exposed metal sites.

Supporting Information Available: Tables of gas sorption data, BET analysis reports, thermogravimetric analysis plots for compounds **3−6**, a plot of the O_2 desorption isotherm for desolvated **6**, and the powder X-ray diffraction pattern of desolvated **6** (PDF); X-ray crystallographic files (CIF). This material is available free of charge via the Internet at http://pubs.acs.org.

JA061716I

(40) (a) Li, D.; Kaneko, K. *Chem. Phys. Lett.* **2001**, *335*, 50−56. (b) Seki, K. *Phys. Chem. Chem. Phys.* **2002**, *4*, 1968−1971. (c) Serre, C.; Millange, F.; Thouvenot, C.; Noguès, M.; Marsolier, G.; Louër, D.; Férey, G. *J. Am. Chem. Soc.* **2002**, *124*, 13519−13526. (d) Kitaura, R.; Fujimoto, K.; Noro, S.; Kondo, M.; Kitagawa, S. *Angew. Chem., Int. Ed.* **2002**, *41*, 133−135. (e) Kitaura, R.; Seki, K.; Akiyama, G.; Kitagawa, S. *Angew. Chem., Int. Ed.* **2003**, *42*, 428−431. (f) Halder, G. J.; Kepert, C. J. *J. Am. Chem. Soc.* **2005**, *127*, 7891−7900. (g) Mellot-Draznieks, C.; Serre, C.; Surblé, S.; Audebrand, N.; Férey, G. *J. Am. Chem. Soc.* **2005**, *127*, 16273−16278. Reviews: (h) Uemura, K.; Matsuda, R.; Kitagawa, S. *J. Solid State Chem.* **2005**, *178*, 2420−2429. (i) Fletcher, A. J.; Thomas, K. M.; Rosseinsky, M. J. *J. Solid State Chem.* **2005**, *178*, 2491−2510. (j) Chen, B.; Liang, C.; Yang, J.; Contreras, D. S.; Clancy, Y. L.; Lobkovsky, E. B.; Yaghi, O. M.; Dai, S. *Angew. Chem., Int. Ed.* **2006**, *45*, 1390−1393.